Circadian pattern and burstiness in human communication activity

Hang-Hyun Jo,[1] Márton Karsai,[1] János Kertész,[1, 2] and Kimmo Kaski[1]

[1]*BECS, School of Science, Aalto University, P.O. Box 12200, FI-00076*

[2]*Institute of Physics and BME-HAS Cond. Mat. Group, BME, Budapest, Budafoki út 8., H-1111*

(Dated: July 21, 2022)

The temporal pattern of human communication is inhomogeneous and bursty, as reflected by the heavy tail distribution of the inter-event times. For the origin of this behavior two main mechanisms have been suggested: a) Externally driven inhomogeneities due to the circadian and weekly activity patterns and b) intrinsic correlation based inhomogeneity rooted deeply in the task handling strategies of humans. Here we address this question by providing systematic de-seasoning methods to remove the circadian and weekly patterns from the time series of communication events. We find that the heavy tails of the inter-event time distributions are robust with respect to this procedure indicating that burstiness is mostly caused by the latter mechanism b). Moreover, we find that our de-seasoning procedure improves the scaling behavior of the distribution.

I. INTRODUCTION

Recently modern information-communication-technology (ICT) has opened us access to large amount of stored digital data on human communication, which in turn enable us to have unprecedented insight into the human behavioral and social patterns. For example we can now study the structure and dynamics of large human communication networks [1–4], the laws of mobility [5–7], as well as the motifs of individual behavior [8–11]. One of the robust findings of these studies is that human activity over a variety of communication channels is inhomogeneous, i.e. bursty, such that bursts of rapidly occurring events of activity are separated by long periods of inactivity. This feature is usually characterized by the distribution of inter-event times τ, defined, e.g., as time intervals between consecutive e-mails sent by a single user. This distribution has been found to have heavy tail and show a power-law decay as $P(\tau) \sim \tau^{-1}$ [8].

In human behavior an obvious cause of inhomogeneity is the circadian and other longer and naturally occurring cycles of our lives. This can be described by inhomogeneous Poisson processes with different characteristic times corresponding to the different cycles, leading to an apparent power-law behavior in the inter-event time distribution as demonstrated by Malmgren *et al.* [9, 10]. They have claimed that the approximate power-law scaling is a consequence of circadian and weekly cycles of human activity, such that the large inter-event times are attributed to nighttime and weekend inactivity. They proposed a cascading inhomogeneous Poisson process, which is a combination of two Poisson processes with different time scales. One of them is characterized by the time-dependent event rate representing the circadian and weekly activity patterns, while the other corresponds to the cascading burst behavior for a shorter time scale. Their model was able to reproduce the heavy-tailed inter-event time distribution.

However, the question remained whether there are also intrinsic correlations that contribute to the inhomogeneities observed in communication patterns, as suggested, e.g., by the queuing models [8, 12]. There is evidence for this by Goh and Barabási [13], who introduced a measure that indicates the communication patterns to have correlations beyond these time cycles. Recently, Wu *et al.* have studied the modified version of queuing process proposed in [8] by introducing a Poisson process as the initiator of localized bursty activity [14]. This is aimed at explaining the observation that the inter-event time distributions in Short Message (SM) correspondence follow a bimodal combination of power-law and Poisson distributions. The power-law (Poisson) behavior was found dominant for $\tau < \tau_0$ ($\tau > \tau_0$). Since the event rates extracted from the empirical data have the time scales larger than τ_0 (also measured empirically), the bimodal distribution is successfully obtained. In their work, the effect of circadian and weekly activity patterns is not considered and thus needing to be investigated in detail.

Our aim in this paper is to apply a de-seasoning method by which the inhomogeneities due to the circadian and weekly patterns can be removed from the data. Then the study of the remaining de-seasoned data would enable us to decide about the existence of intrinsic correlations. This question is important for two reasons. First, communication patterns tell about the nature of human behavior. Second, appropriate modeling should properly take into account the different origins of inhomogeneities: Is it enough to describe the communication pattern by an inhomogeneous Poissonian process or do we need models reflecting the intrinsic correlations in human activities?

In this paper, we provide the method of de-seasoning the circadian and weekly patterns systematically. Firstly, we extract the circadian and weekly patterns from the time-stamped communication records. Secondly, such patterns are removed by rescaling the timings of the communication events, i.e. phone calls and SMs. The rescaling is performed such that the time is dilated (contracted) at times of high (low) activity. Finally, we obtain
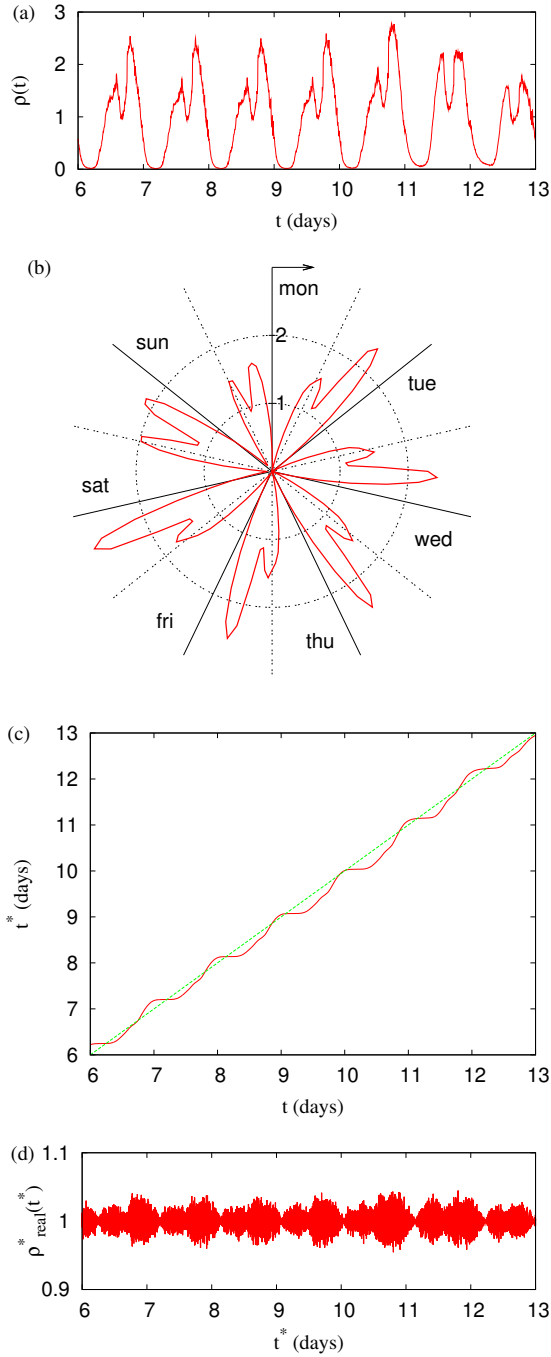
FIG. 1: Mobile phone call (MPC): (a) Homogeneous event rate as a function of real time, $\rho(t)$, shows the circadian and weekly patterns typical in human activity. January 8, 2007 (from 6 to 7 in the plot) is Monday. (b) The event rate averaged over the whole period is visualized in a polar plot where the direction of time is set as the counter-clockwise. (c) The rescaled time as a function of original time, $t^*(t)$. (d) Rescaled event rate, $\rho^*_{\mathrm{real}}(t^*)$, also shows the circadian and weekly pattern.
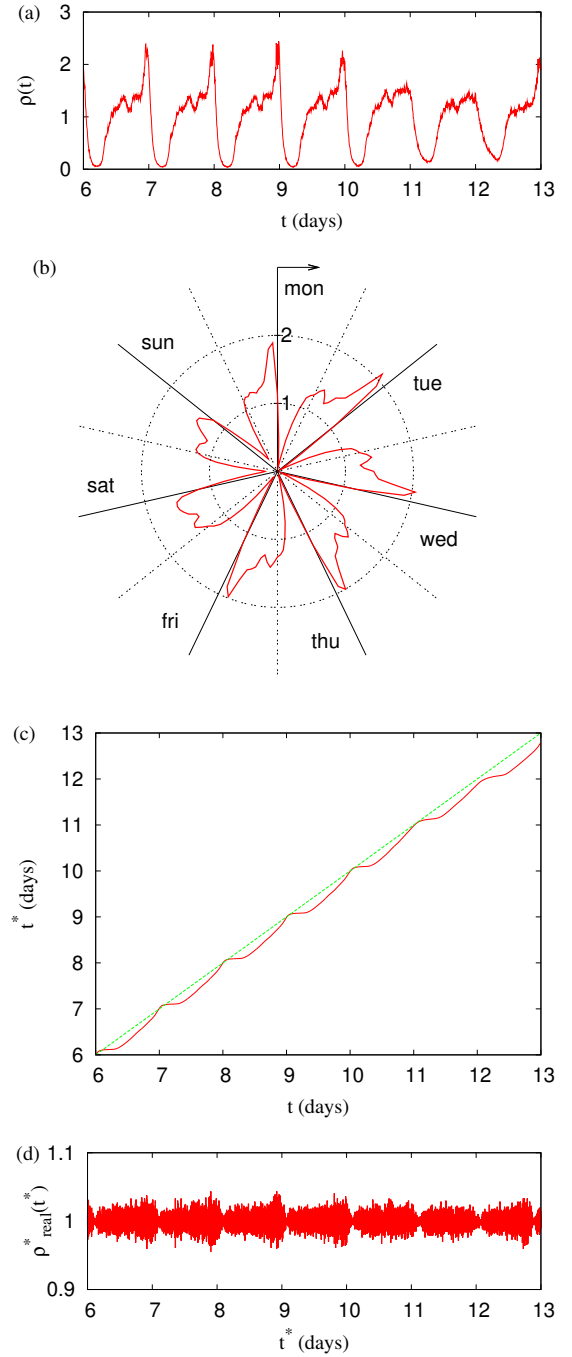
FIG. 2: Short Message (SM): (a) Homogeneous event rate as a function of real time, $\rho(t)$, shows the circadian and weekly patterns typical in human activity. January 8, 2007 (from 6 to 7 in the plot) is Monday. (b) The event rate averaged over the whole period is visualized in a polar plot where the direction of time is set as the counter-clockwise. (c) The rescaled time as a function of original time, $t^*(t)$. (d) Rescaled event rate, $\rho^*_{\mathrm{real}}(t^*)$, also shows the circadian and weekly pattern.

the inter-event time distributions by using the rescaled timings and comparing them with the original distributions to check how the heavy tail and burstiness are affected. We will show that the heavy tail and burstiness are mostly due to intrinsic correlations in human communication patterns.

This paper is organized as follows. In Section II, we introduce methods of de-seasoning the circadian and weekly patterns systematically in various ways. In Section III, the inter-event time distributions are obtained and discussed. Finally, we summarize the results in Section IV.

II. CIRCADIAN AND WEEKLY PATTERNS

We investigate the effect of circadian and weekly cycles on the heavy-tailed inter-event time distribution and burstiness in human activity by using the following data [11]: (a) Mobile phone call (MPC) data and (b) Short Message (SM) data from a European operator (national market share $\sim 20\%$) with time-stamped records over a period of 119 days starting from January 2, 2007. The data of January 1, 2007 are not considered due to its unusual usage pattern. We have only retained links with bidirectional interaction, yielding for the MPC data $N = 5.2 \times 10^6$ nodes (users), $L = 10.6 \times 10^6$ links, and $C = 322 \times 10^6$ events (calls), while for the SM data we have $N = 4.2 \times 10^6$ nodes, $L = 8.5 \times 10^6$ links, and $C = 114 \times 10^6$ events (SMs). We have merged some consecutive SMs sent by one user to another within 10 seconds into one SM event because one longer message can be divided into many short messages due to the length limit of a single SM (160 characters) [15].

As an observable for the circadian and weekly cycles, we define the event density $c(t)$ in real time t. If C_T is the average density over an entire period T, i.e. 119 days, then the rescaled time t^* is defined by

$$dt^* = \frac{c(t)}{C_T} \, dt = \rho(t)dt, \tag{1}$$

where $\rho(t)$ denotes the event rate. This rescaling corresponds to the transformation of the time variable by $\rho^*(t^*)dt^* = \rho(t)dt$ with $\rho^*(t^*) = 1$. Here $\rho^*(t^*) = 1$ means that there exists no cyclic pattern in the frame of rescaled time. The time is dilated (contracted) at the moment of high (low) activity. For convenience, we set $t = 0$ as the start of January 2, 2007 at midnight (Tuesday).

Next we consider the homogeneous and the activity dependent rescaling methods. For the former case, the rescaled time is the same to all nodes, while for the latter case, nodes and links are divided into classes depending on the intensity of their activities. The time of each class is rescaled by means of its own event rate, which is different from class to class.

A. Homogeneous rescaling

From Eq. (1), we obtain the event rate, $\rho(t)$, the corresponding rescaled time, $t^*(t)$, and the rescaled event rate, denoted by $\rho^*_{\text{real}}(t^*)$, for MPC data, depicted in Fig. 1. Here the 7th day ($6 \leq t < 7$ in days) is Monday. We find the characteristic circadian pattern, i.e. inactive nighttime and active daytime with two peaks with one of them in the afternoon and the other in the evening. The event rate indicates two typical but clearly distinguishable circadian patterns, i.e. one for the weekdays and another for weekend days. During the week the peaks in the afternoon are substantially smaller than those in the evening, while the corresponding peaks during weekends are equally high. This could be related to the fact that during the weekday office hours a lot of communication takes place by emails while in the evenings and during weekends communication is more mobile device related. The Friday evening "partying" behavior is represented by the largest peak of the week. It is also found that the activities on Saturdays are stronger than those on Sundays. This circadian and weekly pattern is typical so that it is averaged over the entire period of data to be presented by the polar plot in Fig. 1(b). The rescaled time is obtained by integrating the event rate as shown in Fig. 1(c).

In Fig. 1(d), the rescaled event rate successfully shows the expected de-seasoning effect, i.e. $\rho^*(t^*) = 1$, except for the very weak fluctuation, yielding the deviation $\sigma \approx 0.012$. It is found that not only the event rates but also their fluctuations show the circadian and weekly patterns. The circadian fluctuation has two parts, the stronger one in the late afternoon and the weaker one in the early morning. The weekday fluctuation is again distinguished from the weekend fluctuation. These behaviors imply the higher order structures, which can be attributed to the heterogeneity of the activities of nodes and links. Thus we need to look at the detailed structure of the human activity in social interaction.

In Fig. 2 for SM data, we also find the characteristic circadian and weekly patterns, but with one distinct peak at midnight on weekdays and without it on weekends. This pattern is typical over the entire four months period, studied here. Finally, the circadian fluctuation becomes maximized around midnight. The value of overall deviation is $\sigma \approx 0.011$.

B. Activity dependent rescaling

Here we consider the heterogeneous variation of different activities of nodes and links, separately. It is already well known that the activities of nodes and links in Mobile phone communication are broadly distributed [2]. To be precise, the activity of a node, say u, is defined as the number of events involving that node, denoted by $n^{(u)}$. On the other hand the activity of a link between nodes u and v, is defined as the number of events between them,

TABLE I: Node-activity dependent classification in the MPC records. For each class, the number of nodes, its fraction, the total number of events, its fraction, and the number of events per node are summarized.

class	nodes	%	events	%	events per node
0	2570601	49.5	63548222	9.9	24.7
1	744937	14.4	64332300	10.0	86.4
2	488915	9.4	64132228	10.0	131.2
3	370071	7.1	65521873	10.1	177.1
4	283450	5.5	64453626	10.0	227.4
5	226338	4.4	64466743	10.0	284.8
6	181558	3.5	64406651	10.0	354.7
7	143716	2.8	64136145	10.0	446.3
8	110460	2.1	64711883	10.0	585.8
9	69607	1.3	64622457	10.0	928.4

TABLE II: Link-activity dependent classification in the MPC records. For each class, the number of links, its fraction, the total number of events, its fraction, and the number of events per link are summarized.

class	links	%	events	%	events per link
0	6232153	58.6	30857579	9.6	5.0
1	1787245	16.8	33397645	10.4	18.7
2	878051	8.3	31075239	9.6	35.4
3	579344	5.4	32535169	10.1	56.2
4	393346	3.7	32797666	10.2	83.4
5	270489	2.5	31928005	9.9	118.0
6	199592	1.9	32632312	10.1	163.5
7	142395	1.3	32496984	10.1	228.2
8	96960	0.9	32071110	10.0	330.8
9	55106	0.5	32374355	10.0	587.5

denoted by $n^{(uv)}$.

We classify nodes and links depending on their activities: For the node-activity dependent classification (node-class in short), we divide the set of nodes into 10 classes, where the fraction of events in each class is supposed to be approximately the same:

$$N_q = \{u|\ n_q < n^{(u)} \leq n_{q+1}\} \text{ for } q = 0, \cdots, 9. \quad (2)$$

TABLE III: Node-activity dependent classes in the SM records. For each class, the number of nodes, its fraction, the total number of events, its fraction, and the number of events per node are summarized.

class	nodes	%	events	%	events per node
0	2870595	67.9	22355372	9.8	7.8
1	543943	12.9	22644129	10.0	41.6
2	297703	7.0	22792034	10.0	76.6
3	189676	4.5	23006745	10.1	121.3
4	124702	2.9	22689038	10.0	182.0
5	85017	2.0	22900383	10.1	269.4
6	56080	1.3	22829185	10.0	407.1
7	34714	0.8	22747278	10.0	655.3
8	18762	0.4	22760770	10.0	1213.1
9	7129	0.2	22756058	10.0	3192.0

TABLE IV: Link-activity dependent classes in the SM records. For each class, the number of links, its fraction, the total number of events, its fraction, and the number of events per link are summarized.

class	links	%	events	%	events per link
0	5671344	66.7	10166245	8.9	1.8
1	1601345	18.8	12422285	10.9	7.8
2	574691	6.8	10965758	9.6	19.1
3	311767	3.7	11806863	10.4	37.9
4	160271	1.9	11440639	10.1	71.4
5	88838	1.0	11411312	10.0	128.5
6	49863	0.6	11373634	10.0	228.1
7	27410	0.3	11393087	10.0	415.7
8	13381	0.2	11383857	10.0	850.7
9	4584	0.1	11376816	10.0	2481.9

Here $n_0 = 0$ and n_q with $q > 0$ satisfies

$$\frac{q}{10} = \frac{1}{2C} \sum_{n=1}^{n_q} n|\{u|n^{(u)} = n\}|, \quad (3)$$

where C is the total number of events, see Table I for the MPC data and Table III for the SM data. For MPC (SM) data, about 50% (68%) of all the nodes belong to $q = 0$ class, which seems consistent with the broad scale distribution of node activities. Similarly, we can divide the set of links into 10 classes (link-class in short):

$$L_q = \{uv|\ n_q < n^{(uv)} \leq n_{q+1}\} \text{ for } q = 0, \cdots, 9. \quad (4)$$

Here $n_0 = 0$ and n_q with $q > 0$ satisfies

$$\frac{q}{10} = \frac{1}{C} \sum_{n=1}^{n_q} n|\{uv|n^{(uv)} = n\}|. \quad (5)$$

The details are presented in Table II for the MPC data and in Table IV for the SM data. For the MPC data, the distribution of links over classes is more skewed than that of nodes. Note that the node-class and the link-class schemes cannot be used simultaneously.

For both node-activity and link-activity dependent classifications, we obtain the event rates $\rho_q(t)$ for all q. In the polar plot we also present the pattern ratios, $\rho_q(t)/\rho(t)$, to compare the event rate of each class with the homogeneous event rate, $\rho(t)$. The characteristic circadian pattern, i.e. inactive nighttime and active daytime, is clearly visible in all cases. However, we observe different fine structures depending on the activity of the class.

For the node-class case of the MPC data in Fig. 3(a) and (c), the most inactive class $q = 0$ shows overall less activity compared to the homogeneous weekly pattern, i.e. $\rho_0(t) < \rho(t)$, and exceptionally weak activity for daytimes on weekends, implying $\rho_0(t) \gtrsim \rho(t)$. Such deviation from the homogeneous event rate tends to vanish for the moderately active classes up to $q = 6$. The most active class $q = 9$ shows strong nighttime activity, especially on
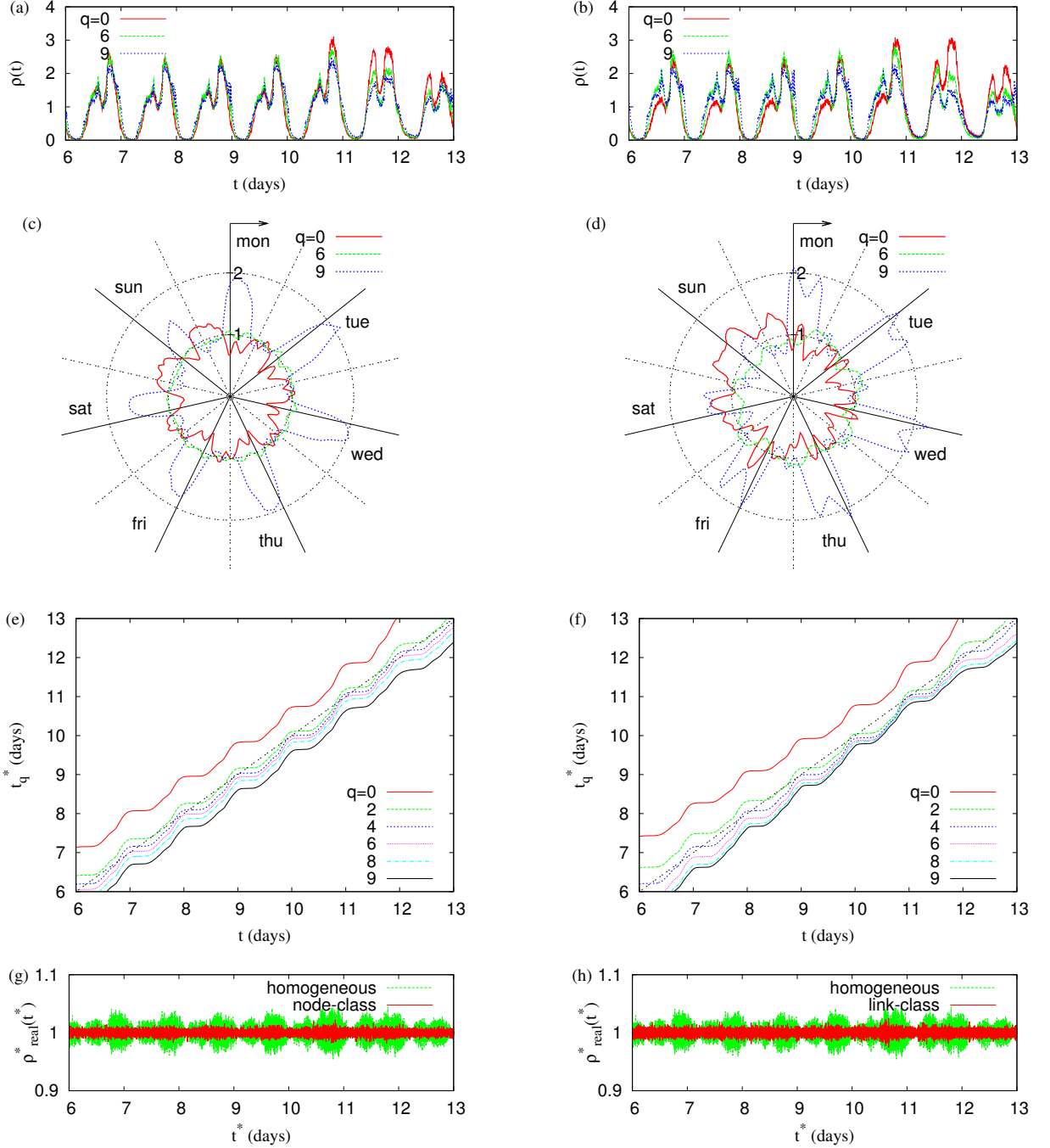
FIG. 3: MPC analysis with node-activity (left) and link-activity (right) dependent classifications. (a)-(b) q-class event rates, $\rho_q(t)$, show the overall similar circadian and weekly patterns but with different higher order structures. (c)-(d) Their ratios to the homogeneous event rate, $\rho_q(t)/\rho(t)$, are visualized in a polar plot as in Fig. 1(b). (e)-(f) q-class rescaled times, $t_q^*(t)$. (g)-(h) Rescaled event rates, $\rho_{\rm real}^*(t^*)$, in both node-class and link-class cases fluctuate much less than the homogeneous case.

weekdays, and weak daytime activity, especially on weekends. For the link-class case we find qualitatively similar behavior in Fig. 3(b) and (d) as in the node-class case. The different behaviors are observed for the most inactive classes. For the class $q = 0$, the activity especially from 2 am to 5 am seems rather neutral, $\rho_0(t) \approx \rho(t)$, and this

class shows the activity in nighttime on weekends.

How can we understand these differences? The active nodes may have active links as well as inactive links. On the other hand, the inactive nodes are much less likely to have active links. As a result, the cyclic patterns of active links are highly correlated with those of active nodes.
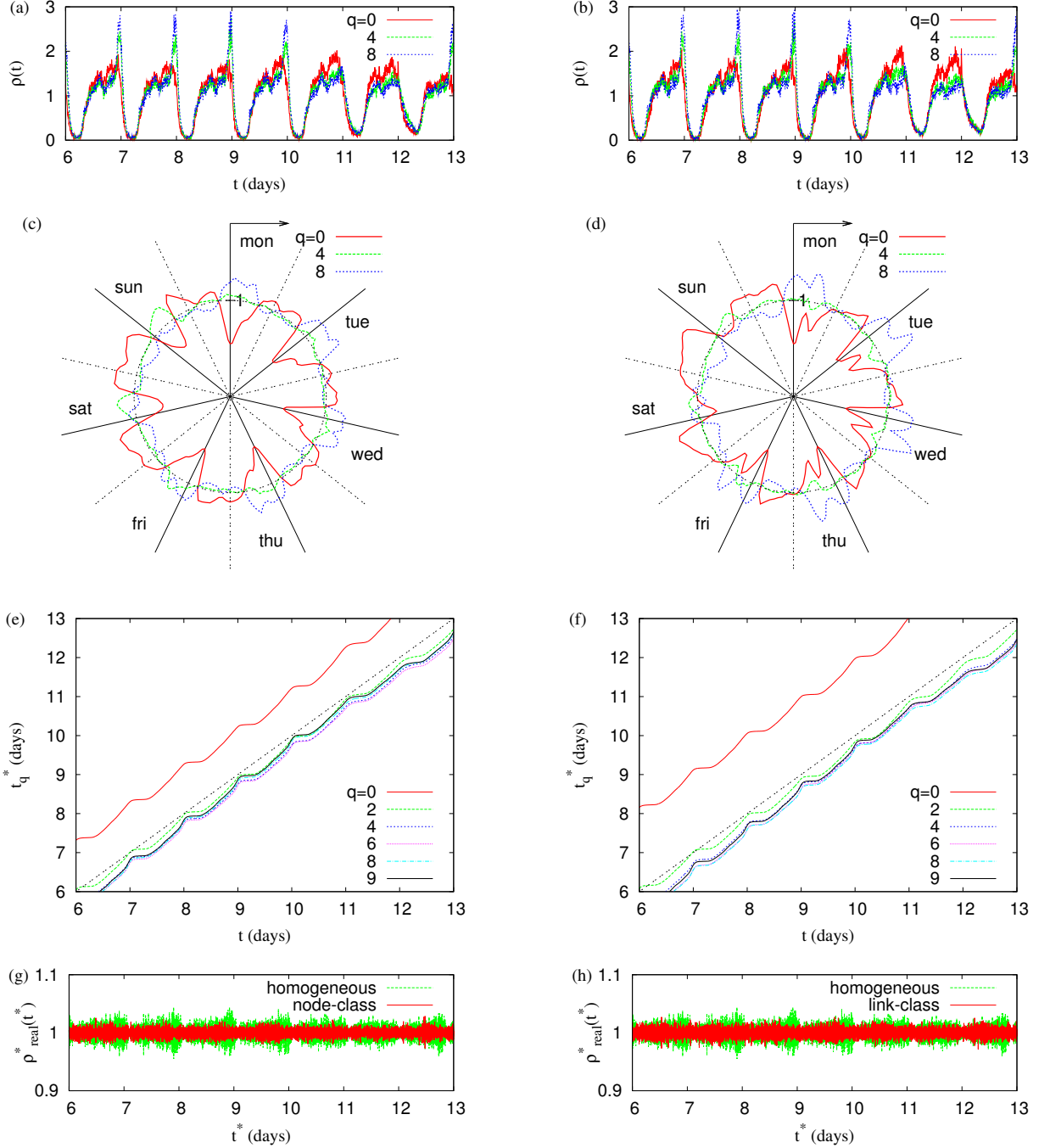
FIG. 4: SM analysis with node-activity (left) and link-activity (right) dependent classifications. (a)-(b) q-class event rates, $\rho_q(t)$, show the overall similar circadian and weekly patterns but with different higher order structures. (c)-(d) Their ratios to the homogeneous event rate, $\rho_q(t)/\rho(t)$, are visualized in a polar plot as in Fig. 2(b). (e)-(f) q-class rescaled times, $t_q^*(t)$. (g)-(h) Rescaled event rates, $\rho_{\mathrm{real}}^*(t^*)$, in both node-class and link-class cases fluctuate less than the homogeneous case.

The patterns of inactive links are not only correlated with those of inactive nodes but also affected by those of active nodes. Thus, the behaviors of inactive node-classes and of the inactive link-classes can be different. The different event rates from class to class are taken into account by rescaling times separately, see Fig. 3(e)-(f).

Next, we proceed by putting the rescaled timings of events together, the rescaled event rates are obtained for node-class and for link-class, respectively. They are compared with the rescaled event rate of the homogeneous case in Fig. 1(d). As expected, the fluctuation becomes weaker and closer to the white noise than in the homoge-
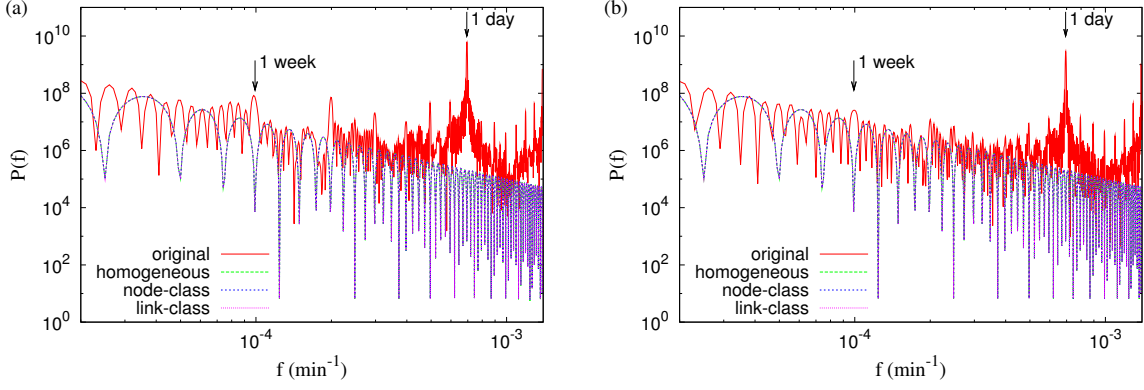
FIG. 5: Power spectra, $P(f)$, of the original and rescaled event rates (a) for MPC and (b) for SM. The circadian and weekly peaks in the original power spectrum are successfully removed by the de-seasoning in various ways.

neous case, see Fig. 3(g)-(h). To be precise, the deviation is 4.9×10^{-3} for node-class and 5.4×10^{-3} for link-class, which was 0.012 for the homogeneous case. So we can conclude that the de-seasoning is improved due to taking higher order structures into account.

The results for SM data are shown in Fig. 4. Contrary to the MPC results, it turns out that the peaks at midnight on weekdays are not contributed by the inactive classes. For node-class case, the most inactive class $q = 0$ shows very weak nighttime and strong daytime activity every day, as compared to the homogeneous event rate. The very active class $q = 8$ shows strong activity from the late evening to the early morning on weekdays and weak activity otherwise. The most active class $q = 9$ shows the characteristic behavior such that the nodes in this class are more active at nighttime than those of class $q = 8$ (not shown). We observe similar behavior in the link-class case. In summary, the aggregated activities in the SM data can be decomposed into classes better than those in the MPC data. The rescaled event rates fluctuate around 1, as expected, see Fig. 4(g)-(h). The deviations are decreased to 6.0×10^{-3} in the node-class case and 6.9×10^{-3} in the link-class case due to considering higher order structures in human activity.

In order to see clearly the effect of de-seasoning on the event rates, we compare the power spectra of the rescaled event rates to the original event rates. The power spectrum of the event rate is defined as

$$P(f) = \left| \int_0^T \rho(t) e^{2\pi i f t} dt \right|^2, \qquad (6)$$

where f denotes the frequency. In Figure 5 we show the results of this comparison, where it is evident that with our de-seasoning methods, discussed above, the circadian and weekly peaks of the original power spectrum are successfully removed and do not show in the rescaled spectra for both the MPC and SM time-series. However, as can be seen by detailed inspections of Fig. 3(g) and (h) and of Fig. 4(g) and (h), both the node- and link-

activity dependent rescalings are able to improve the de-seasoning results by large amount over the homogeneous de-seasoning results.

III. BURSTINESS

In order to check whether our rescalings affect the inter-event distributions and whether still some intrinsic correlations due to burstiness exists we have reformulated the inter-event time distributions by using rescaled event timings and compare them with the original distributions. The definition of the rescaled inter-event time from the rescaled time is straightforward. Considering two consecutive events of a node (or a link) occurring at times t_j and t_{j+1}, the original inter-event time is $\tau_j \equiv t_{j+1} - t_j$ then for the homogeneous rescaling method, the corresponding rescaled inter-event time is defined as follows

$$\tau_j^* \equiv t^*(t_{j+1}) - t^*(t_j) = \int_{t_j}^{t_{j+1}} \rho(t') dt'. \qquad (7)$$

In the case of activity dependent rescaling, the inter-event time is similarly defined as above, but with $\rho(t)$ replaced by $\rho_q(t)$ for each activity class q. Once the rescaled times of nodes in the node-activity dependent classification are obtained, the rescaled times of links can be defined by means of rescale times of nodes, and vice versa. However, the definition of inter-event time is no longer straightforward for a link whose end nodes belong to different classes and thus have different rescaled times corresponding to the same original time. Here we resolve this uniqueness dilemma by simply taking the average of the rescaled times of the two nodes, say u and v, as the rescaled time of the link, say uv:

$$t^{*(uv)}(t) \equiv \frac{1}{2}[t^{*(u)}(t) + t^{*(v)}(t)] \qquad (8)$$

for any t. If, however, nodes u and v belong to the same class, we get uniquely $t^{*(uv)}(t) = t^{*(u)}(t) = t^{*(v)}(t)$. On
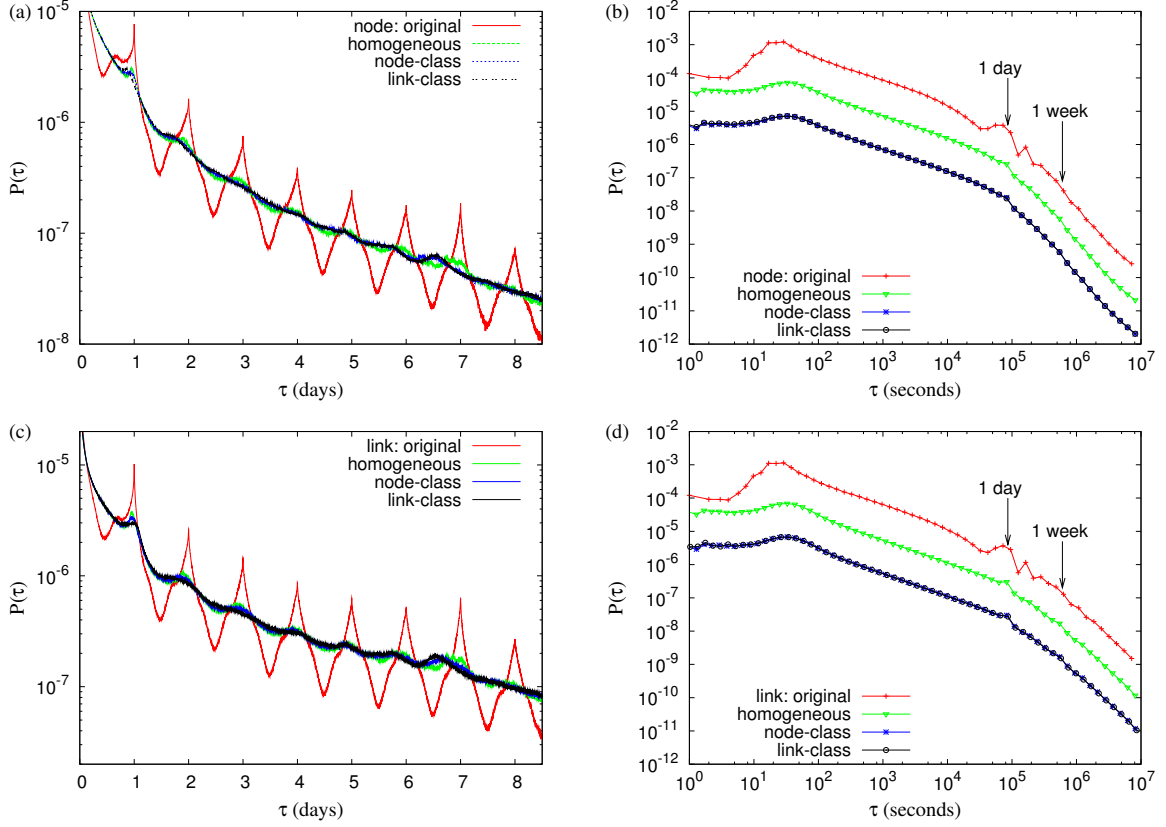
FIG. 6: MPC: Semi-log (left) and log-log (right) plots of original and rescaled inter-event time distributions for nodes (top) and for links (bottom). In the log-log plots, the node-class and the link-class curves are shifted downwards for the clear presentation. In all cases, the circadian peaked structures in the original distributions have clearly disappeared and the scaling behaviors are improved and become more apparent having performed the de-seasonings.

the other hand, we can obtain the rescale times of links in the link-activity dependent classification and then the rescaled times of nodes by means of those of links. In some case, however, the order of events of one node can be reversed if those events occur on the links belonging to different classes and thus having different rescaled times. To get around this issue we take the average of rescaled times of links attached to one node as the rescaled time of that node:

$$t^{*(u)}(t) \equiv \frac{1}{|\Lambda_u|} \sum_{v \in \Lambda_u} t^{*(uv)}(t), \qquad (9)$$

where Λ_u denotes the set of node u's neighbors. We have chosen these definitions for computational simplicity among many other possible ones.

Regarding to the inter-event times, we like to remark upon the boundary effect of the time domain studied here. All the nodes (users) we took into account subscribed before January 1, 2007 and had not unsubscribed by April 30, 2007. If a user made his/her first call the February 1, we count one month as the inter-event time until that call, and if a user made his/her call the April 1 and did not call by the end of April, we count one month as the inter-event time from that call. However, when

defining the inter-event time of a link, we do not count the former (from January 1 to the first event February 1) but the latter (from the last event April 1 to April 30). This is because if two nodes never knew each other before April 1 and then talked over the phone on that day for the first time, we cannot claim that they 'waited' for making a call for three months. On the other hand, if two nodes talked over the phone the March 1 and did not call until the end of April, we can count this case as the inter-event time of that link.

In Fig. 6 and Fig. 7 we present the original and the rescaled inter-event time distributions for nodes and links for all the cases considered above. In case of the original distributions of the MPC data there exists one hump located around at $\tau = 16$ hours and a series of 'circadian' peaks at $\tau = d$ days with natural number d. The heights of circadian peaks decreases as d increases, except for the 'weekly' peaks at $\tau = w$ weeks with natural number w, whose heights also decrease as w increases. In all the rescaled inter-event time distributions, the hump has been smoothed out and the circadian peaks have been suppressed very effectively but not completely. This is partly because the circadian pattern within each day is de-seasoned successfully. However, since the circadian
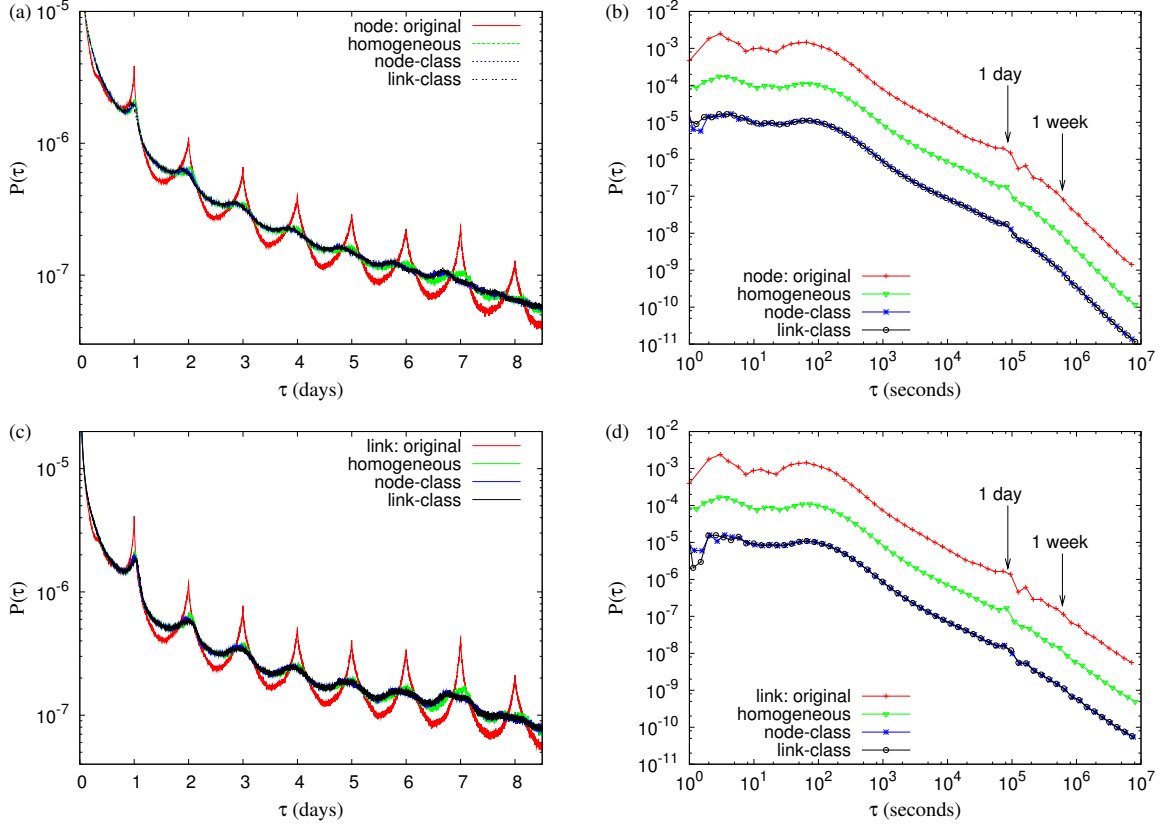
FIG. 7: SM: Semi-log (left) and log-log (right) plots of original and rescaled inter-event time distributions for nodes (top) and for links (bottom). In the log-log plots, the node-class and the link-class curves are shifted downwards for the clear presentation. In all cases, the circadian peaked structures in the original distributions have been suppressed and the scaling behaviors are improved having performed the de-seasonings.
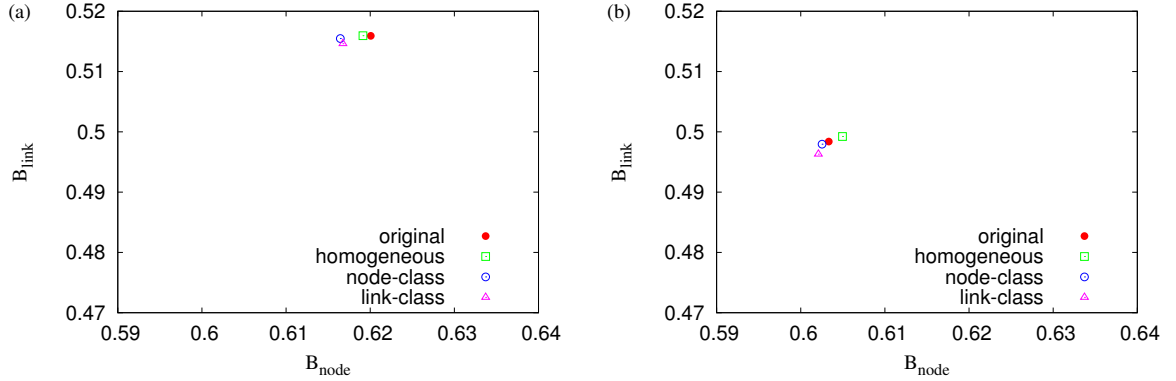

FIG. 8: The node and link burstinesses of original and rescaled inter-event time distributions (a) for MPC data and (b) for SM data. The burstinesses turn out to be weakly affected by the de-seasoning.

patterns for different days are more or less similar, the inter-event times close to the multiples of one day barely change. From these figures we can see that from the rescaling schemes we have used here, overall the link-class rescaling method shows the best performance. It is also observed that the suppressed weekly peaks moved their positions to the smaller values of τ. Finally, should

we like to suppress the seasonal peaks even more, we should consider also the higher order structures in the data, like the somewhat different phone usage patterns between weekdays and weekends.

Now we are in the position to check the power-law scaling behavior by log-log plotting the original and rescaled inter-event time distributions of the MPC data

in Fig. 6. In all the cases we observe one scaling regime of $\tau < \tau_\times \approx 1$ day and the apparently heavy tails for the range of $\tau > \tau_\times$. However, we cannot conclusively say whether the tail has another scaling regime or just indicates the exponential cutoff. The first scaling regime is characterized by $P(\tau) \sim \tau^{-\alpha}$ with $\alpha \approx 0.7$, which agrees with that by Karsai *et al.* [11]. Furthermore, we observe that the scaling behavior remains after performing the de-seasonings of the circadian and weekly patterns. In fact, the first scaling regime has been extended to the larger τ region and the quality of scaling has been improved, which is mainly due to the suppressed circadian peaks. Therefore, one can say that the heavy tails and burstiness in human activity are not the consequence of circadian and weekly cycles, but really existing. For the second regime, the tails of distributions for links shown in Fig. 6(b) and in Fig. 7(b) are heavier than those for nodes as shown in Fig. 6(d) and in Fig. 7(d). This is rooted to the fact that the inter-event time of a link, say uv, can be generally written as the sum of consecutive inter-event times of one involved node, say u.

For the inter-event time distributions of SM data presented in Fig. 7, we find the overall similar behavior as presented for the MPC data. We note that there is no peaks around $\tau = 16$ hours, and that the scaling regime of $2 \times 10^3 < \tau < 2 \times 10^4$ is characterized by $P(\tau) \sim \tau^{-\alpha}$ with $\alpha \approx 1$, even though the scaling regime is not larger than one decade. By de-seasoning the scaling regime has been extended to about 1.5 decades. Also in this case, we cannot conclusively say whether there is a second scaling regime for $\tau > \tau_\times$ or it is an indication of a cutoff.

In order to find out how much the de-seasoning affects burstiness, we measure the burstiness of events and the memory between consecutive events, as proposed in [13]. The burstiness parameter B is defined as

$$B \equiv \frac{\sigma_\tau - m_\tau}{\sigma_\tau + m_\tau}, \qquad (10)$$

where σ_τ and m_τ are the standard deviation and the mean of inter-event time distribution $P(\tau)$, respectively. The value of B is bounded in the range of $(-1, 1)$ such that $B = 1$ for the most bursty behavior, $B = 0$ for neutral behavior, and $B = -1$ for a completely regular behavior. One can obtain burstiness of the nodes and links, denoted by B_{node} and B_{link}, from inter-event time distributions of nodes and links, respectively. In

Fig. 8 the burstinesses of original and rescaled distributions are represented by the points in the $(B_{\text{node}}, B_{\text{link}})$-space. All points are located in a very narrow region, implying that the burstiness is weakly affected by de-seasoning for both MPC and SM data. This observation supports our conclusion about the heavy tails and burstiness being independent of the circadian and weekly patterns. We have also measured the memory coefficient of inter-event times, defined as the autocorrelation function $\langle (\tau_j - m_\tau)(\tau_{j+1} - m_\tau) \rangle / \sigma_\tau^2$, and confirmed that the memory is not affected by the de-seasoning effect (not shown).

IV. SUMMARY

We have provided the method of systematically de-seasoning circadian and weekly patterns in human activity to figure out the issue whether the heavy tails and burstiness are the consequence of such seasonal patterns or the intrinsic correlation based inhomogeneity rooted in the task handling strategies of humans. The circadian and weekly patterns extracted from the mobile phone call and Short Messages records are used to rescale the timings of events, i.e. the time is dilated (contracted) during high (low) call or SM activity of users. We have also considered higher order structures in human activity by classifying nodes and links depending on their activities.

We have found that after de-seasoning human activity patterns, the heavy tails and burstiness of inter-event time distributions still remain. Furthermore, the scaling behavior has been improved due to suppressing circadian peaks in the tails of distribution. Our results imply that the heavy tails and burstiness are not simply the consequence of circadian and weekly cycles, but due to the intrinsic correlation based inhomogeneity.

[1] J.-P. Onnela, J. Saramäki, J. Hyvönen, G. Szabó, D. Lazer, K. Kaski, J. Kertész, A.-L. Barabási, Proc. Natl. Acad. Sci. (USA) **104**, 7332 (2007).

[2] J.-P. Onnela, J. Saramäki, J. Hyvönen, G. Szabó, M.A. de Menezes, K. Kaski, A.-L. Barabási, J. Kertész, New J. Phys. **9**, 179 (2007).

[3] G.M. Krings, F. Calabrese, C. Ratti, V.D. Blondel, J. Stat. Mech. L07003 (2009).

[4] G. Palla, A.-L. Barabási, T. Vicsek, Nature **446**, 664 (2007).

[5] C. Song, Z. Qu, N. Blumm, A.-L. Barabási, Science **327**, 1018 (2010).

[6] C. Song, T. Koren, P. Wang, A.-L. Barabási, Nat. Phys. **7**, 713 (2010).

[7] M.C. González, C.A. Hidalgo, A.-L. Barabási, Nature **453**, 779 (2008).

[8] A.-L. Barabási, Nature **435**, 207 (2005).

[9] R.D. Malmgren, D.B. Stouffer, A.E. Motter, L.A.N.

Amaral, Proc. Nat. Acad. Sci. **105**, 18153 (2008).

[10] R.D. Malmgren, D.B. Stouffer, A.S.L.O. Campanharo, L.A.N. Amaral, Science **325**, 1696 (2009).

[11] M. Karsai, M. Kivelä, R.K. Pan, K. Kaski, J. Kertész, A.-L. Barabási, J. Saramäki, arXiv:1006.2125v3 (2010).

[12] A. Vázquez, J.G. Oliveira, Z. Dezső, K.-I. Goh, I. Kondor, A.-L. Barabási, Phys. Rev. E **73**, 036127 (2006).

[13] K.-I. Goh and A.-L. Barabási, EPL **81**, 48002 (2008).

[14] Y. Wu, C. Zhou, J. Xiao, J. Kurths, H.J. Schellnhuber, Proc. Nat. Acad. Sci. doi: 10.1073/pnas.1013140107 (2010).

[15] L. Kovanen, Master's Thesis, *Structure and dynamics of a large-scale complex social network*, Aalto University (2009).